Title

Lapsed El Niño impact on Atlantic and Northwest Pacific tropical cyclone activity in 2023.

Permalink

https://escholarship.org/uc/item/87h3n99s

Journal

Nature Communications, 15(1)

Authors

Zhao, Jiuwei

Zhan, Ruifen

Wang, Yuqing

et al.

Publication Date

2024-08-07

DOI

10.1038/s41467-024-51241-9

Peer reviewed

Lapsed El Niño impact on Atlantic and Northwest Pacific tropical cyclone activity in 2023

Jiuwei Zhao [1], Ruifen Zhan [2] ✉, Yuqing Wang [3] ✉, Shang-Ping Xie[4], Leying Zhang[5] & Mingrui Xu[2]

A typical El Niño event often results in suppressed tropical cyclone (TC) genesis frequency (TCGF) over the North Atlantic (NA) and a distinct northwest-southeast dipole pattern in TCGF anomaly over the western North Pacific (WNP). The 2023 saw a strong El Niño event but surprisingly active NA and suppressed WNP TC activities. Here, we present that these unprecedented deviations were driven by the record-warm NA, a record-breaking negative phase of the Pacific Meridional Mode (PMM), and background global warming. Results from high-resolution global model experiments demonstrate that extraordinary Atlantic warming dominated the increased NA TCGF and contributed equally with the PMM to the suppressed WNP TCGF, overshadowing El Niño's impact. Global warming also contributed to the observed TCGF anomalies. Our findings demonstrate that the typical influence of strong El Niño events on regional TC activity could be markedly altered by other climate modes, highlighting the complexity of TC genesis in a warming world.

The 2023 tropical cyclone (TC) season in the North Atlantic (NA) and western North Pacific (WNP) was unprecedented and peculiar. From June to November, the NA witnessed the formation of 20 TCs, the third highest since 1980, trailing only the 2005 and 2020 seasons. In contrast, the WNP experienced a marked reduction in TC frequency across the entire basin, with only 13 TCs observed, approximately 9 fewer (-2 standard deviation) than the climatological mean of 21.6 for the 1980-2023 period, tying with the lowest (third) number of TCs based on the TC best-track data from the United States (China or Japan) since 1980. The 2023 season is uncommon also in that the NA surpasses the WNP in annual counts by a large margin. Thus, the 2023 TC season holds considerable significance due to its unusual nature.

What makes this even more unusual is that the year 2023 was the developing year of a strong El Niño[1]. The 2023 El Niño event, based on the June-November (JJASON) averaged sea surface temperature (SST)

anomaly, ranks as the fifth strongest since 1980 (Supplementary Fig. 1). It is well documented in previous studies that a strong El Niño suppresses TC genesis over the NA[2] due to the strengthening of the local vertical wind shear. The concurrent El Niño impact is insignificant on the WNP basin count, manifested instead as a spatial redistribution with suppressed TC genesis frequency (TCGF) in the northwestern but increased TCGF in the southeastern part of the WNP[3,4] (Supplementary Fig. 1). The deviations from the expected impact of a strong El Niño on NA and WNP TC activities in 2023 mark the first occurrence of genesis frequency since the inception of TC records, representing a lapsed El Niño impact on NA and WNP TC genesis in 2023 (Supplementary Fig. 2). As a result, the TC season in either basin was not well predicted in the early seasonal forecasts (https://www.cpc.ncep.noaa.gov/products/outlooks/hurricane2023/May/Slide1.JPG and https://www.weather.gov/gum/2023WestPacTropicalCycloneOutlook).

[1]Collaborative Innovation Center on Forecast and Evaluation of Meteorological Disasters (CIC-FEMD), Institute for Climate and Application Research (ICAR), Nanjing University of Information Science & Technology (NUIST), Nanjing, China. [2]Department of Atmospheric and Oceanic Sciences & Institute of Atmospheric Sciences, Fudan University, Shanghai, China. [3]Department of Atmospheric Sciences and International Pacific Research Center, School of Ocean and Earth Science and Technology, University of Hawaii at Manoa, Honolulu, HI, USA. [4]Scripps Institution of Oceanography, University of California San Diego, La Jolla, CA, USA. [5]College of Ecology and Environment, Joint Innovation Center for Modern Forestry Studies, Nanjing Forestry University, Nanjing, China. ✉e-mail: zhanrf@fudan.edu.cn; yuqing@hawaii.edu

In addition to the El Niño-Southern Oscillation (ENSO), a number of other factors may affect TC activity over the NA and WNP (Supplementary Fig. 2b). From the difference in SST between 2023 and average of other four strong El Niño events, the SST anomaly over the tropical North Atlantic (TNA) can be considered as an important factor in modulating inter-basin TCGF, inducing a seesaw change between the NA and WNP basins[5–8]. Positive TNA SST anomalies can promote local TC genesis over the NA while suppress TC activity over the WNP through modulating atmospheric circulation. Previous studies[9–15] have also highlighted the influence of the Pacific Meridional Mode (PMM) on WNP TCGF with its negative phase suppressing TC genesis, which is well shown in Supplementary Figs. 2b and 3 with the strong negative SST anomaly over the subtropical eastern Pacific. It is worthy to note that while previous studies[16,17] have separately investigated the impacts of the PMM and TNA on WNP and NA TCGFs, their combined effects and relative contributions alongside global warming (GW) and ENSO across basins remain unknown. The complexity of spatial SST anomalies in 2023 necessitates an integrated analysis of these modes. Here, we verified that the PMM and TNA have significant impacts on TCGF over the eastern part of the WNP (E_WNP; 140°E-180°), while their influences are weak on TCGF over the western WNP (W_WNP; 100°-140°E; Supplementary Fig. 4). The Indian Ocean SST anomalies in 2023 show a significant dipole pattern (Supplementary Fig. 5), indicating a strong positive Indian Ocean Dipole phase[18,19]. However, since the Indian Ocean Dipole is not significantly correlated to TCGF anomalies, it was not featured in the following discussion. Additionally, basin-dependent changes in TCGF have been observed in response to GW[20–22], with the NA TCGF experiencing an upward trend, whereas the WNP TCGF shows a decreasing trend (Supplementary Fig. 6a). Moreover, this inter-basin seesaw change in TCGF is highly corresponded with the La Niña-like SST warming pattern and is consistent with the trends of circulations (Supplementary Fig. 6b–e). Therefore, it strongly suggests that the mean-state warming impact on TCGF over the WNP and NA is nonnegligible in 2023 (Supplementary Fig. 7). Comparing with the other four El Niño events, the GW tends to contribute to the increased NA TCGF and the suppressed WNP TCGF in 2023 (Supplementary Fig. 7c, f).

The PMM index averaged during JJASON in 2023 has reached a record-breaking low value since 1980, at -2.03 standard deviation (Supplementary Figs. 3 and 4). Meanwhile, a record-breaking warming was observed in the NA, surpassing 2.5 (3.1) standard deviation with the long-term linear warming trends excluded (included). These extraordinary circumstances may have played a vital role in shaping the unprecedented TC season over the NA and WNP in 2023, leading to the lapsed El Niño impact, which might differ significantly from previous years due to their extreme nature. The primary objective of this study is to untangle the underlying physical causes responsible for the lapse of El Niño impact on TCGF over the NA and WNP in 2023, and to quantify the relative contributions of the corresponding key factors.

Results

Lapsed El Niño impact on TC genesis in 2023

Previous studies[2,3] have extensively documented the suppressive effect of strong El Niño on TC genesis over the NA, while inducing a distinct negative-positive dipole pattern in TCGF anomalies over the northwestern (western) and southeastern (eastern) parts of the WNP (contours in Fig. 1a, b; Supplementary Fig. 1). However, the anticipated impact of El Niño was nullified in 2023. Figure 1a shows an anomalous increase in TCGF over most of the tropical Atlantic with an increase of over 4.0 in the middle of the basin, while a slight decrease in the coastal and Caribbean regions. This pattern accounts for the fact that among the 20 TCs, only 3 TCs (Idalia, Ophelia, and Lee) made landfall in such an active season. Remarkably, the WNP experienced a shift from the dipole pattern of TCGF anomaly to a basin-wide decrease (Fig. 1b; shaded). As a result, this basin witnessed the lowest TCGF since 1980,

with only 13 TCs formed during JJASON in 2023. The other lowest TCGF year for the WNP was 2010, characterized by a strong La Niña event following a strong El Niño in the previous winter[23]. Hence, a question arises as to why the anticipated El Niño impact on NA and WNP TCGF was strongly deviated from the observed pattern in 2023.

To address this question, we turn to other oceanic factors/modes in addition to ENSO (Supplementary Fig. 8a). Adjacent to the prominent positive SST anomaly of El Niño are a negative SST anomaly over the subtropical eastern North Pacific and a positive anomaly over the tropical Atlantic. The former represents the negative phase of the PMM[24–28] (Supplementary Fig. 8b). Intriguingly, the JJASON-averaged PMM index in 2023 displays a record-breaking low value, reaching -2.03 standard deviation from the 1980 baseline. The negative PMM typically drives an anticyclonic circulation anomaly over the North Pacific and equatorial easterly wind anomalies over the WNP, significantly suppressing WNP TC genesis (Fig. 1b). Coincidentally, the TNA[5,7,29] in 2023 also reaches record-breaking warming, at 2.5 (3.1) standard deviation with (without) the removal of the long-term linear trends of SSTs (Supplementary Fig. 8c). The positive TNA SST anomaly is beneficial to local TC genesis over the NA (Fig. 1a), but unfavorable for TC genesis over the WNP (Fig. 1b). In addition to the three interannual modes mentioned above (ENSO, PMM and TNA), global SST warming exhibits a La Niña-like warming pattern since 1980[20,22,30] (Supplementary Fig. 8d), characterized by accelerated warming in the NA, WNP and Indian Ocean, but a relatively smaller warming trend in the central-eastern Pacific. This La Niña-like warming pattern, accompanied with tropical divergent wind anomalies, is consistent with recent increasing trend of TCGF over the NA (Fig. 1c; black line). Referring to the La Niña-like GW pattern, we further defined the GW index as the global average of JJASON SST from 1980 to 2023.

We further calculated the correlations of TCGF with ENSO, PMM and NA SST indices (Fig. 1e, f and Supplementary Figs. 3 and 4). The NA TCGF exhibits a significant negative correlation with the Niño3.4 index ($r = 0.38$; note that the Niño3.4 index is reversed), while a significant positive correlation with the local SST anomalies in the TNA ($r = 0.66$; Fig. 1e). The correlation coefficient reaches 0.76 based on a multi-regressed model using ENSO, PMM, TNA and GW indices. Additionally, we have compared the TNA index with the Atlantic Meridional Mode[31–33], which has been acknowledged as an important factor modulating NA TCGF. A highly significant correlation between them was found. Upon removing the linear trends from both time series, the correlation weakens moderately, indicating a partial contribution of GW. The relationship between WNP TCGF and the Niño3.4 index is overall insignificant, but it becomes significant in two subregions corresponding to the dipole pattern of TCGF during different ENSO phases (Supplementary Fig. 4e, f). In particular, we found strong correlations of WNP TCGF with both the reversed PMM/TNA index and regression model ($r = 0.52/0.52$ and $r = 0.64$, respectively). Therefore, we hypothesize that the lapse of El Niño impact on the NA and WNP TCGF in 2023 may be attributed to the PMM, the TNA SST anomaly, and GW.

Causes of the unprecedented TCGF anomalies over the NA and WNP in 2023

To test the above hypothesis, we first reconstructed the SST anomalies in 2023 through combining the four factors/modes including El Niño, negative PMM, positive TNA, and global SST warming based on the linear regression method. To ensure the robust regression results, we further employed two approaches to calculate the regression coefficients (See Method). The first approach involved a sample-independent regression model (Fig. 2), while the other approach utilized regressed SST anomalies multiplying normalized coefficients for reconstruction (Fig. 3b). The sample-independent regression model reasonably captures the spatially uniform increase in NA TCGF and decrease in WNP TCGF (Fig. 2c, d), as well as the record-breaking high
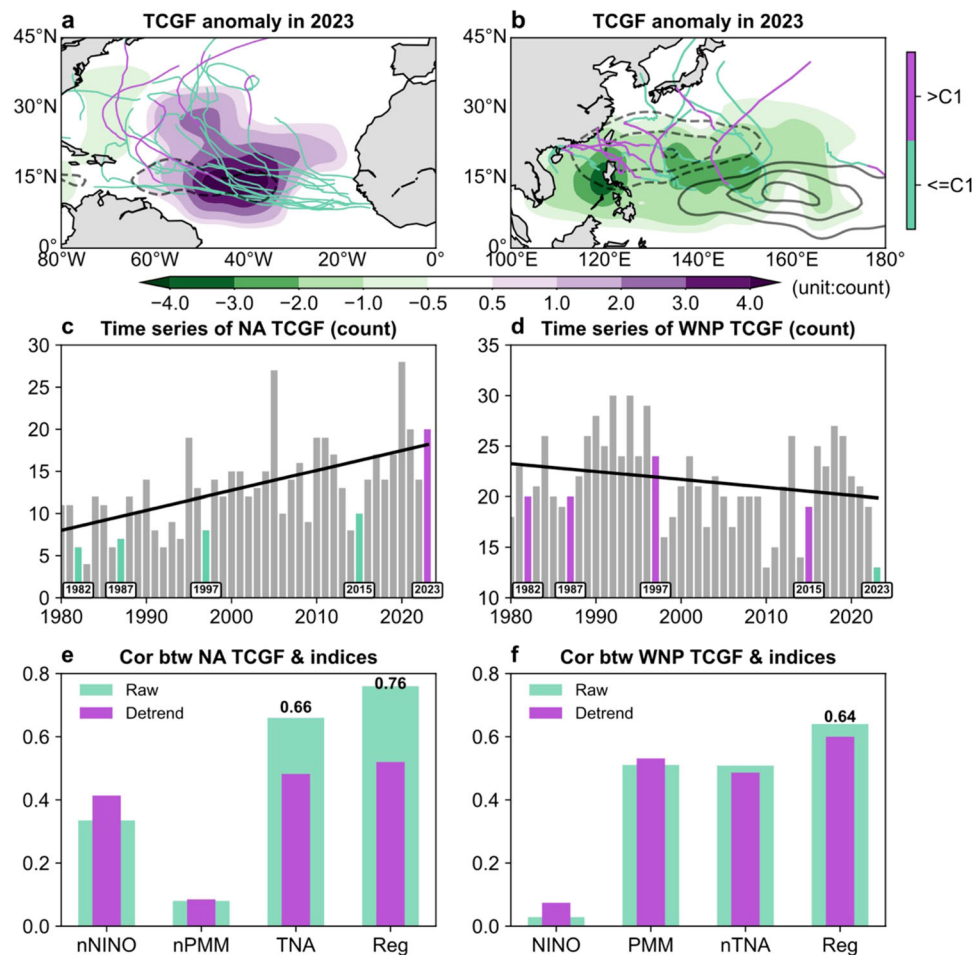
Fig. 1 | Spatial and temporal tropical cyclone genesis frequency (TCGF; unit: count), and correlation with the controlling factors. a North Atlantic (NA) TCGF anomaly in 2023 (shaded) and composite of TCGF anomaly for top four El Niño events (1982, 1987, 1997 and 2015; contour); (b) same as (a) but for the western North Pacific (WNP); (c) time series of NA TCGF from 1980 to 2023; (d) time series of WNP TCGF; (e) correlations between NA TCGF with respective reversed Niño [Niño × (-1)], reverted Pacific Meridional Mode (PMM) index [PMM × (-1)], tropical North Atlantic (TNA) index and multi-regressed (Reg) TCGF based on above three indices and the global warming (GW) index based on the 1980–2023 period; and (f) correlations between WNP TCGF with respective Niño, PMM, reverted TNA [TNA × (-1)] index and multi-regression result for 1980–2023 period. The 2023 TC tracks in (a, b) are shown in green and purple colors that the green represents TC intensity is smaller than Category 1 (C1) while the purple means the intensity is above C1. The black contours in (a, b) stand for the composite of TCGF anomalies between positive and negative ENSO phases with positive values using solid lines and negative using dashed lines. The values range from −3 to 3 with zero line neglected. The green and purple bars in (c) and (d) represent the five strong El Niño years with the green bars representing low TCGF year while purple bars for high TCGF year. The "Reg" represents correlations between TCGF and multi-regressed TCGF based on TNA, PMM, ENSO and GW indices. Here, the green bars stand for correlation coefficients with the un-detrended TCGF while the purple bars are for the detrended TCGF.

TCGF in the NA and the unusually low in the WNP (Fig. 2e, f). The results based on the two approaches are generally consistent with each other. It is noteworthy that the PMM and ENSO are orthogonal to each other (with correlation coefficient $r = -0.09$). Moreover, the JJASON-averaged TNA SST exhibits an insignificant simultaneous correlation ($r = 0.04$) with ENSO, suggesting their mutual independence. The magnitude of GW is adjusted to minimize the variance between the reconstructed and observed SST anomalies (See Method). As a result, the bias between the observed and reconstructed SST anomalies is 0.37 °C from 45°S to 45°N and 0.2 °C from 15°S to 15°N. The reconstructed atmospheric circulation response well reproduces the robust anticyclonic circulation anomaly over the North Pacific (Fig. 3a vs Fig. 3b; and Supplementary Fig. 9a), which is responsible for the decrease in WNP TCGF in 2023 (Fig. 1). Additionally, the anomalous cyclonic circulation, accompanied by strong equatorial westerly wind anomalies over the NA, is also effectively reproduced. This circulation pattern can be attributed to both local Atlantic warming and global SST warming, thereby leading to an increase in NA TCGF. When the El

Niño impact is intentionally excluded, strong easterly wind anomalies persist over the WNP, while westerly wind anomalies prevail over the NA, indicating the consistent impacts on TCGF in both basins with the reconstructed SST anomalies, irrespective of the inclusion of El Niño (Fig. 3c and Supplementary Fig. 9b). The circulation patterns remain similar when the influence of global warming is not considered, albeit with the reduced magnitude (Fig. 3d and Supplementary Fig. 9c). Furthermore, the circulation patterns remain similar to those in response to the observed and the reconstructed SST anomalies when only the PMM and the TNA are considered (Fig. 3e and Supplementary Fig. 9d). It strongly suggests that the PMM and the TNA played a critical role in controlling TCGF across both basins in 2023.

Further, we conducted a series of sensitivity experiments based on a high-resolution global atmospheric model[34–36] (See Method). In these experiments, SST in the model was prescribed to the SSTs observed in 2023, albeit with some modifications. To ensure robustness, we conducted 30 ensemble simulations, each with different initial conditions that were perturbed with a small magnitude, for all
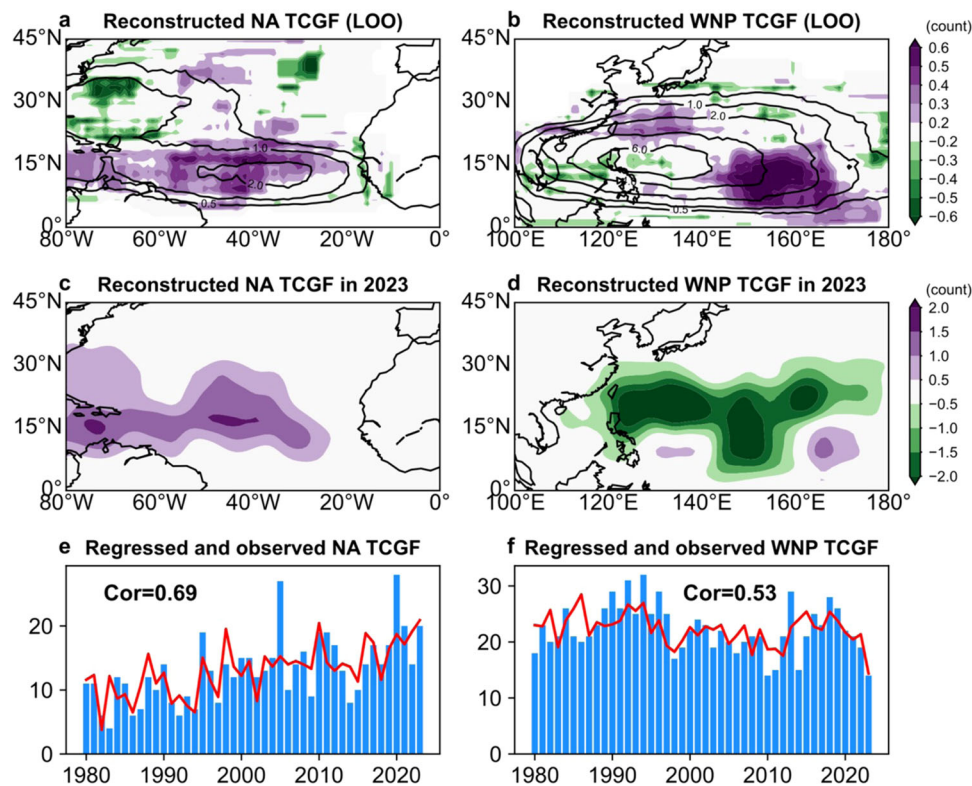
Fig. 2 | Regressed tropical cyclone genesis frequency (TCGF; unit: count) based on Leave-One-Out (LOO) Method. a Spatial correlations (shaded) between the observed and regressed North Atlantic (NA) TCGF based on LOO method at each grid point; (**b**) same as (**a**) but for the western North Pacific (WNP) TCGF; (**c**) predicted TCGF in 2023 over the NA based on the tropical North Atlantic (TNA), Pacific Meridional Mode (PMM) and El Niño-Southern Oscillation (ENSO) and global warming (GW) indices using the cross-validated regression model; (**d**) same as (**c**) but for the WNP TCGF; (**e**) observed (bar) and regressed TCGF summed for the whole NA basin based on the cross-validated regression model; and (**f**) same as (**e**) but for the WNP TCGF. The black contour in (**a**, **b**) represent the climatological TCGF.

experiments. In the first experiment, referred to as the CLIM Run, we restored the SST to the climatological monthly mean SST averaged over the period 1980–2022. In the second experiment, called the All Run, we prescribed the SST to that observed in 2023. The CLIM and All Runs yielded 9.8 and 17 TCs over the NA, and 24.5 and 17.7 TCs over the WNP, respectively. These values were close to those observed for both the climatology and the 2023 season. Moreover, the pattern of the simulated TCGF anomaly in All Run from the CLIM Run (Fig. 4a, b; contours) mirrored the observed TCGF anomaly over the NA and the WNP in 2023 (Fig. 1a, b), with an overall increase over the NA and a decrease over the WNP. The fidelity of the TCGF simulations by the high-resolution global model gave us confidence in conducting further sensitivity experiments using the model. In the third experiment, called the Reconstruction Run, we added SST anomalies composed by El Niño (Supplementary Fig. 8a), negative PMM (Supplementary Fig. 8b), positive TNA (Supplementary Fig. 8c), and global warming (Supplementary Fig. 8d) in 2023 to the climatological SST as the oceanic boundary condition (See Method). The differences between the Reconstruction and CLIM Runs are generally consistent with those between All and CLIM Runs (Fig. 4a, b; contours vs shades), indicating that the reconstructed SST anomalies based on the four oceanic modes (negative PMM, positive TNA, El Niño and GW) can reproduce the unprecedented TCGF anomalies over the NA and WNP in 2023.

Relative contributions of oceanic modes to TCGF anomalies in 2023

The above analysis has revealed the fundamental factors/modes driving the unprecedented TCGF anomalies over the NA and WNP in 2023. The relative contributions of those key factors/modes were evaluated

by conducting a series of sensitivity experiments. The No_ElNiño and No_GW Runs were identical to the Reconstruction Run except that the El Niño SST anomaly and the linear trend increments of SST were removed, respectively. The PMM Run, TNA Run, and PMM_TNA Run were identical to the CLIM Run but with the negative PMM anomaly, positive TNA SST anomaly, and both added onto the CLIM SST, respectively.

With the 2023 El Niño SST anomaly removed, the TCGF anomalies over the NA and WNP still exhibited a similar pattern to the Reconstruction/ALL Run, albeit with slight difference in the magnitudes in both basins (Fig. 4a, b). Without the El Niño influence, the NA TCGF experienced a greater increase, while the TCGF over the southeastern part of the WNP underwent a further decrease (Fig. 4c, d). Conversely, with the GW impact removed (NO_GW Run; Fig. 4e, f), the increase in NA TCGF and the decrease in WNP TCGF weakened compared to those in the Reconstruction Run. Furthermore, the relative importance of PMM and TNA in affecting TCGFs was found to differ in magnitude of TCGF over the NA and WNP (Supplementary Fig. 10).

The relative importance of the key factors/modes is further quantified through box-and-whisker plots (Fig. 5). Compared with the CLIM Run, in Reconstruction Run, the number of TCs in the NA was about 7.2 (6.9 in observation) more (Fig. 5a; CLIM vs Reconstruction Runs), whereas that in the E_WNP was 5.9 (5.1 in observation) less (Fig. 5b; CLIM vs Reconstruction Runs). Specifically, artificially disregarding the El Niño impact in 2023 resulted in a further 34.7% increase in the NA TCGF (Fig. 5a; 3.4 more than that in the Reconstruction Run compared with 9.8 in CLIM), indicating that the El Niño attributes -34.7% to the NA TCGF. However, TCGF over the whole WNP basin is less affected by the El Niño due to its dipole pattern (Fig. 5c;
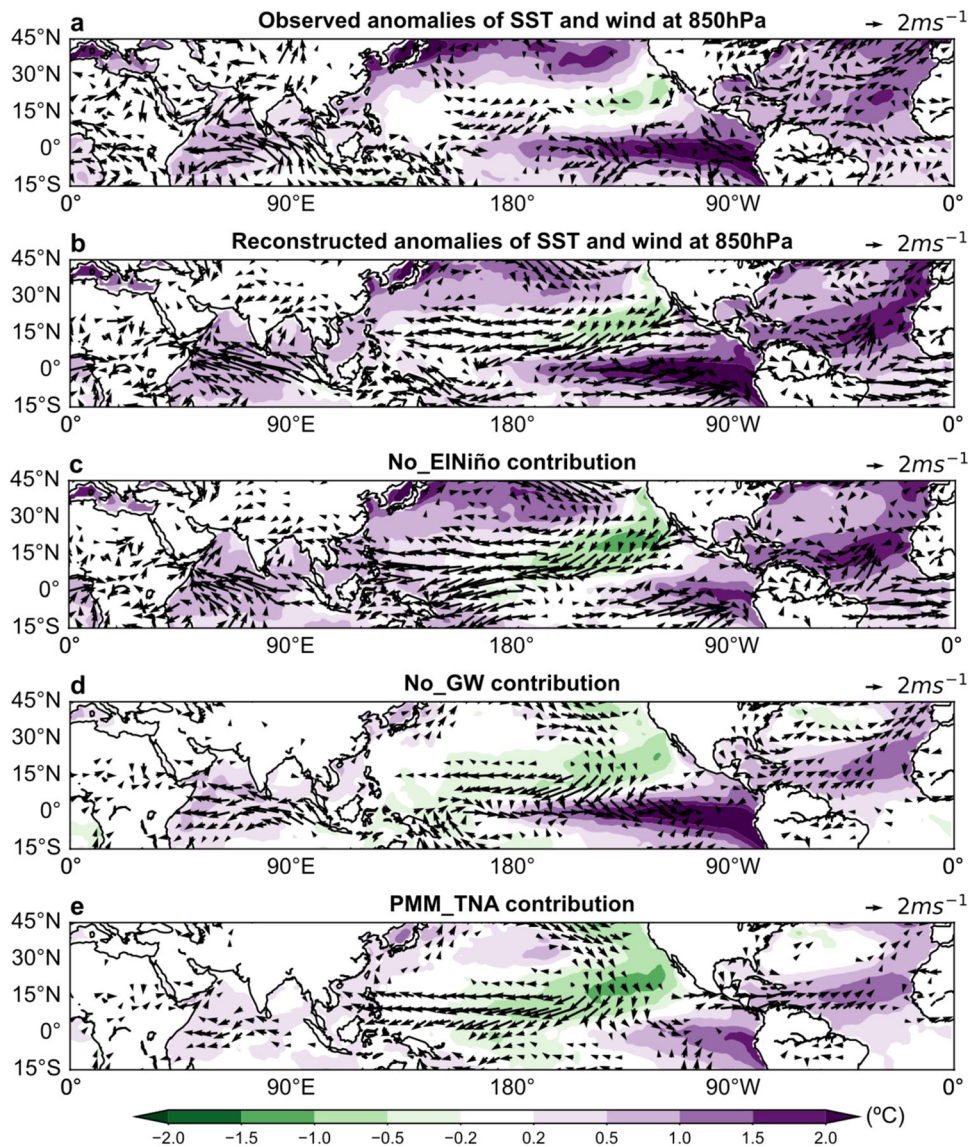
Fig. 3 | Observed and reconstructed wind (unit: m s⁻¹) and sea surface temperature (SST; unit: °C) anomalies. a Low-level wind and SST anomalies in 2023 based on the climatology from 1980 to 2023; (**b**) reconstructed wind and SST anomalies based on Pacific Meridional Mode (PMM) (-2), tropical North Atlantic (TNA) (2.5), El Niño-Southern Oscillation (ENSO) (1.59) and global warming (GW) modes; (**c**) reconstructed wind and SST anomalies based on PMM, TNA and GW; (**d**) reconstructed wind and SST anomalies based on PMM, TNA and ENSO; (**e**) reconstructed wind and SST anomalies based on PMM and TNA. The wind anomalies only with the magnitude large than 0.8 m s⁻¹ are shown.

Reconstruction Run vs No_ElNiño Run). The GW contributed 4.3 (about 43.8%) to the increase in the NA TCGF but 3.6/3.1 (or 14.7%/18.5%) to the decrease in the WNP (E_WNP) TCGF (Fig. 5a, c). Therefore, the GW may offset the suppressive impact of El Niño on NA TCGF, a trend also indicated by the weakening impact of El Niño over time (Fig. 1c). It is worthy to note that both the PMM and TNA have very limited influence on TCGF over the western WNP (W_WNP, 100°–140°E; Supplementary Fig. 4 and Fig. 5d), while they have a prominent impact on TCGF over the eastern WNP (E_WNP, east of 140°E, Fig. 5b). They contributed 42.9% to the decrease in the WNP TCGF and 92.9% increase to the NA TCGF. We find that the TCGF over the E_WNP would decrease more significantly in the absence of the El Niño event in 2023, while it would increase if the GW impact were removed (Fig. 5b; No_ElNiño/No_GW vs CLIM Runs). We also explored the individual and combined contributions of the negative PMM and positive TNA phases. The combined contribution of the PMM and TNA to the NA TCGF was about equal to that in the Reconstruction/All Run. This is likely because the impacts of

El Niño and GW on the NA TCGF had largely offset each other (Fig. 5a). The local TNA SST anomaly is more important for TC genesis over the NA than the SST anomaly over the subtropical eastern Pacific. Both the negative PMM and positive TNA contributed to the suppressed TCGF over the E_WNP with the TNA exerting a relatively more important impact (Fig. 5b).

Discussion
A strong El Niño event often results in the suppressed TCGF over the NA and a northwest-southeast dipole pattern in TCGF anomaly over the WNP. However, the strong El Niño year 2023 presented an intriguing departure with an unexpected active TC season over the NA and an overall decrease in TCGF over the WNP. We found that this significant deviation was primarily due to the record-warm NA, the record-breaking negative phase of the PMM, and the mean state warming. Results from high-resolution model experiments demonstrate that the record Atlantic warming in 2023 dominated the increase
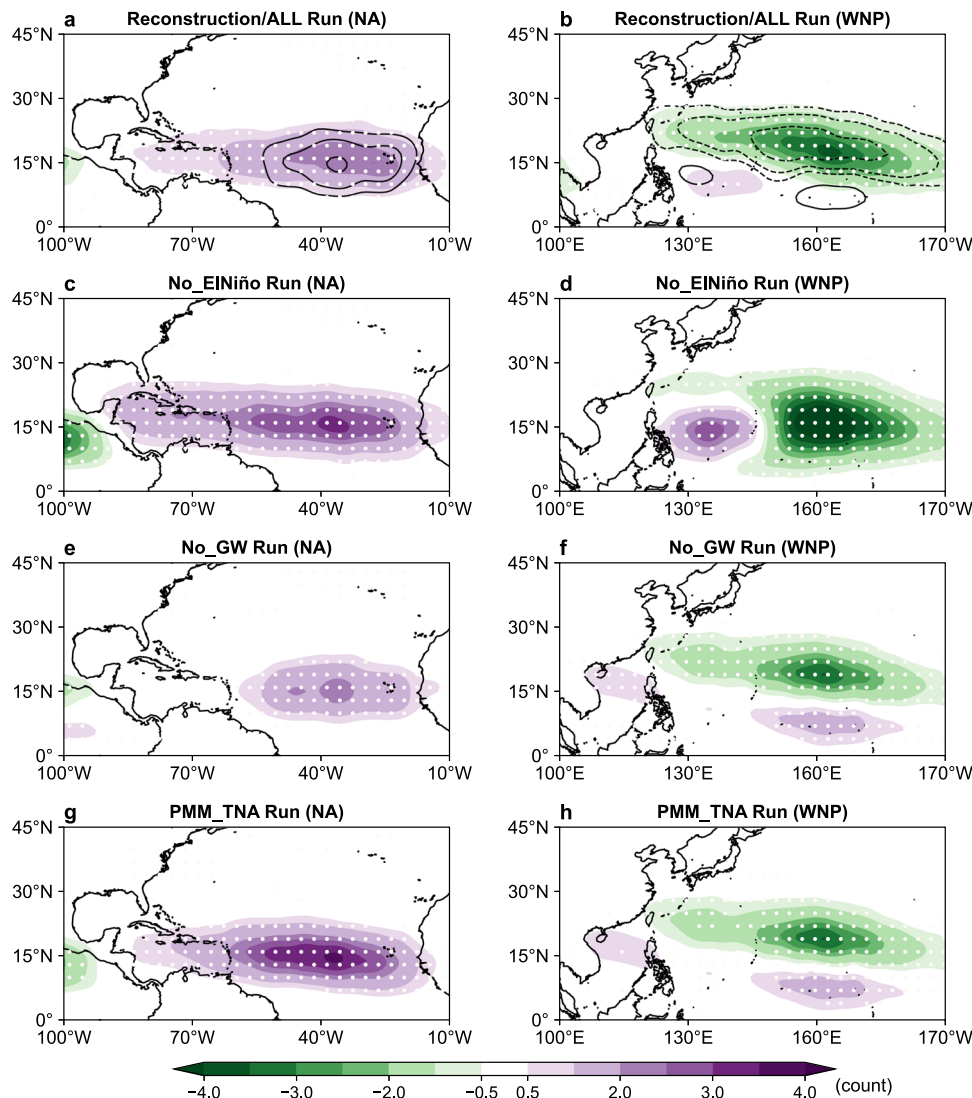
Fig. 4 | Tropical cyclone genesis frequency (TCGF; unit: count) anomalies in different scenarios. a The North Atlantic (NA) TCGF anomaly for reproducing the 2023 situation (TCGF difference between Reconstruction/ALL Run and Clim Run); (**b**) the western North Pacific (WNP) TCGF difference for reproducing the 2023 situation; (**c**) the NA TCGF anomaly for not considering the El Niño impact; (**d**) same as (**c**) but for the WNP TCGF anomaly; (**e**) the NA TCGF anomaly for not considering the GW impact; (**f**) same as (**e**) but for the WNP TCGF anomaly; (**g**) the NA TCGF anomaly for only considering the Pacific Meridional Mode (PMM) and tropical North Atlantic (TNA) impact; and (**h**) same as (**g**) but for the TCGF anomaly. The white dots represent areas above 90% confidence level based on two-tailed Student's t-test. The contour in (**a**, **b**) represents the TCGF difference between All Run and Clim Run while the shading stands for the difference between Reconstruction and CLIM simulations. The contours in (**a**, **b**) range from −3 to 3 at interval of 1 with the zero-contour omitted for clarity. Here, All Run used the observed SST anomalies in 2023 while the Reconstruction Run utilized the reconstructed SST anomalies based on four oceanic modes.

in NA TCGF and equally contributed to the suppression of the WNP TCGF as the PMM, while the global warming contributed positively but secondarily over the WNP and largely suppressed the influence of strong El Niño on the NA TCGF.

Although the TCGF over the eastern North Pacific tends to be above normal in El Nino years, there were 18 TCs in 2023, two fewer than the climatology. This might be due to the negative PMM[11,17]. Here we did not consider the potential impact of the Indian Ocean, although an extremely strong Indian Ocean Dipole was observed in 2023. Limited evidence from previous studies suggested some moderate modulation of TC activity over the WNP by the Indian Ocean Dipole[37]. It is worthy to note that the NA TCGF during the four strongest El Niño events (1982, 1987, 1997, 2015) is below the linear trend line while the 2023 case is above the linear trend line. Whether this implies a weakening impact of El Niño on NA TCGF (Fig. 1c) is a topic for future investigation. Also note that the TCGF in All/Reconstruction Run

shows a systematic northeastward shift of negative TCGF anomaly compared with the observation, which could affect the quantification for the WNP TCGF decrease in some degree. The simulation fails to reproduce the large negative anomalies of TCGF over the South China Sea, which could be largely related to the atmospheric internal variability[4] that the simulation uncertainty can easily grow over the South China Sea due to the warm mean state and degrade the simulation skill of TCGF over the coastal region[38], Nevertheless, we mainly discussed and quantified the TCGF change over the eastern part of the WNP, where the TCGF is significantly modulated by the ENSO, TNA, PMM and GW in 2023 and well captured in the ensemble simulations.

On decadal time scale, the Interdecadal Pacific Oscillation[35,39,40] (IPO) shifted to a negative phase in 1998 and the Atlantic multidecadal Oscillation[41] (AMO) is in its positive phase since 1998. These decadal modes affect the 2023 TC activity marginally through the GW trend.
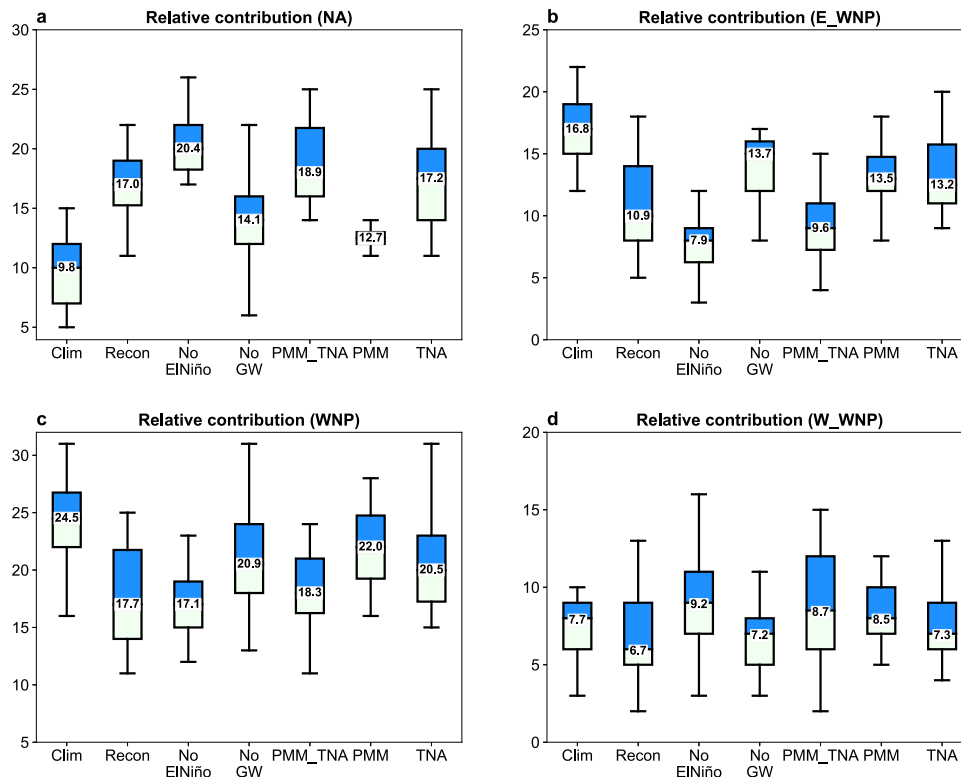
Fig. 5 | Relative contributions of factors to the tropical cyclone genesis frequency (TCGF; unit: count) change. a Box-and-whisker plot of North Atlantic (NA) TCGF for different sensitive experiments; and (**b**) Box-and-whisker plot of TCGF over the east part of the western North Pacific (E_WNP; 140°E-180°) for different sensitive experiments, **c** Box-and-whisker plot of WNP TCGF (100°E–180°) for different sensitivity experiments; and (**d**) Box-and-whisker plot of TCGF over the west part of the western North Pacific (W_WNP; 100°–140°E) for different sensitivity experiments. The values of ± 1.5 stanadard deviation, median, 75th and 25th percentile TCGF are shown in the plots.

Finally, it is important for further exploration into future interannual variability of TC genesis amidst GW. This study underscores sway of oceanic modes over TCGF changes through local environmental alterations, such as tropical westerly wind anomalies, relative vorticity, and vertical wind shear (Fig. 6 and Supplementary Fig. 11). Intriguingly, GW amplifies conditions conducive to TC formation in the NA by enhancing westerly winds and vorticity while reducing wind shear, thus diminishing El Niño's modulatory capacity. Conversely, in the WNP, El Niño's influence shifts TC genesis locations, with GW potentially exacerbating vertical wind shear, suggesting a future decrease in TC activity. The increased variability of TC genesis in both basins during neutral ENSO years, particularly under GW, heralds a future with more pronounced extremes in TC activity, challenging the seasonal predictive reliability in a warming world.

Methods
Best-track TC data and reanalysis dataset
In this study, the best-track TC data, containing 6-hourly TC center (longitude and latitude) and intensity (maximum-sustained surface wind) information during 1980–2023, were derived from the International Best Track Archive for Climate Stewardship (iBTrACS)[42,43]. The TC genesis location was defined when its surface wind speed first reached or exceeded 35 knots (about 17.2 m s^{-1}) during its lifespan. The TC number over the respective NA and WNP basins was calculated based on the boreal summer season from June to November (JJASON). To assess the ranks of WNP TC number in 2023 from the iBTrACS, we also used the TC datasets from the Shanghai Typhoon Institute of China Meteorology Agency (STI/CMA) and the Japan Meteorological Agency (JMA). The 2023 TC number over the WNP in iBTrACS, which was originally from the Joint Typhoon Warning Center (JTWC), is the

lowest since 1980, while it is the second and third lowest based on the datasets from STI/CMA and JMA, respectively.

We used the monthly atmospheric data, such as 850 hPa winds, from the fifth-generation European Centre for Medium-Range Weather Forecasts (ECMWF-ERA5[44]) and National Centers of Environmental Predictions (NCEP)[45] with a horizonal resolution of 2.5°. The monthly SST data were derived from the Hadley Centre Sea Ice and Sea Surface Temperature (HadISST[46]) with a horizontal resolution of 1° × 1°.

Definitions of climate indices
The ENSO was defined as the average of JJASON SST from HadISST over the Niño3.4 region (5°S–5°N; 120°–170°W) for 1980–2023. The Niño index was the normalized time series of ENSO with a weak linear trend removed. The PMM index was downloaded from https://psl.noaa.gov/data/timeseries/monthly/PMM/pmmsst.data. As introduced on the website, the spatial pattern of the PMM was derived from the first mode of singular value decomposition using the SST with both the annual cycle and ENSO signal removed, indicating its relatively independent influence from ENSO ($r = -0.09$). The TNA index was defined as the normalized time series of JJASON-averaged SST over the tropical North Atlantic (EQ–20°N; 10°–60°W) with the linear trend removed. This index shows a minimal correlation with ENSO ($r = 0.04$) but a relatively weak correlation with PMM ($r = -0.4$). In 2023, the normalized Niño3.4 index is 1.59, which is the fifth highest since 1980 (the other four are in 1982, 1987, 1997 and 2015), while the PMM index is the lowest (−2.03) and the TNA value is the highest (+ 2.5). The time series of GW index is normalized based on the global mean JJASON SST from 1980 to 2023. Further, the GW pattern was identified by analyzing the spatial distribution of linear trends of SSTs at each grid point during 1980–2023, revealing a La Niña-like warming pattern (Supplementary
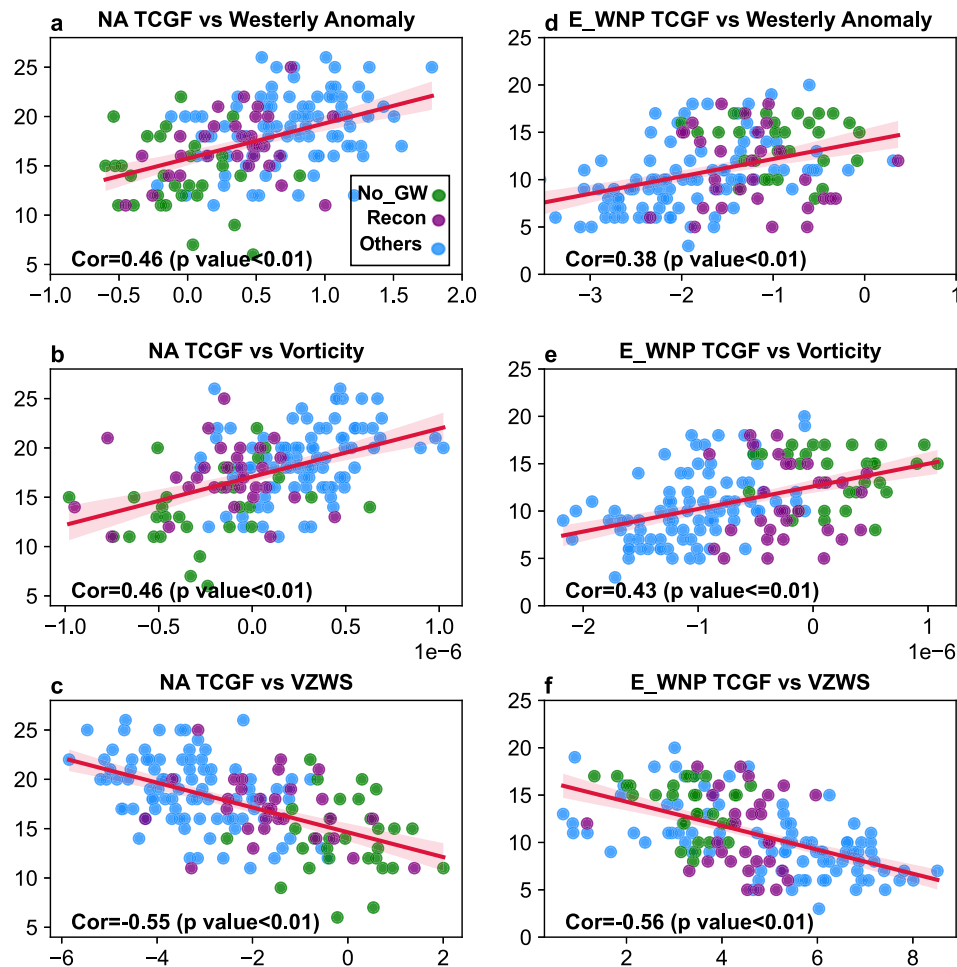
Fig. 6 | Tropical cyclone genesis frequency (TCGF) in response to circulation anomalies forced by different oceanic modes. a–c Scatter plots of North Atlantic (NA) TCGF and (**a**) westerly wind anomalies (unit: m s⁻¹) averaged over 5°S-15°N; 10°-70°W, (**b**) 850 hPa relative vorticity anomalies (unit: 10^{-6} s⁻¹) averaged over the 5°-30°N; 10°-70°W, and (**c**) vertical zonal wind shear (VZWS; unit: m s⁻¹) between 200 hPa and 850 hPa averaged over 0°-15°N; 10°-70°W. **d–f** Scatter plots of TCGF over the east part of the western North Pacific (E_WNP) and (**d**) westerly wind anomalies (unit: m s⁻¹) averaged over 5°S-15°N; 140°E-180°, (**e**) 850 hPa relative vorticity anomalies (unit: 10^{-6} s⁻¹) averaged over the 5°-30°N; 140°E-180°, and (**f**)

vertical zonal wind shear (VZWS; unit: m s⁻¹) between 200 hPa and 850 hPa averaged over 0°-15°N; 140°E-180°. The JJASON-averaged anomalies of wind, vorticity and VZWS are derived from the different between Sensitive (PMM, TNA, PMM_TNA, No_ElNiño, No_GW and Reconstruction) Runs and Clim Run. The correlation coefficient between TCGF and circulation anomalies, and significance level are marked in each subplot. The green dots indicate results from the No_GW experiment, the purple dots from the Reconstruction Run, and the blue dots from the other 4 (PMM, TNA, PMM_TNA and No_ElNiño) Runs that do not contain the El Niño signal.

Fig. 8d). We further checked an extended period from 1960 to 2023 and a more recent period from 1990 to 2023. These analyses reinforced a La Niña-like GW trend pattern (Supplementary Fig. 12).

Model description and TC detection algorithm

In this study, all sensitivity experiments were based on the high-resolution atmospheric model (HiRAM) from the Geophysical Fluid Dynamics Laboratory[34,35,47] (GFDL). The HiRAM model has a horizontal resolution of approximately 50 km and 32 vertical levels, which is capable of explicitly simulating TC-like vortices. Previous studies[22,34] have well documented that the HiRAM can well capture the seasonal and interannual variabilities of TCGF over the NA and WNP.

The 6-hourly outputs from HiRAM, including sea level pressure, 850 hPa winds and vorticity, and the temperature averaged between 500 hPa and 300 hPa, were utilized to derive the TC vortices. The TC detection algorithm was downloaded from GFDL website (https://www.gfdl.noaa.gov/tstorms/), which matches with the HiRAM used in this study and has been widely used in previous studies. The basic detection criteria and steps are as follows: First, there appeared a low-pressure center on the surface. Considering that the TC intensity was

initially weak with considerable asymmetric structure, the surface isobars could not be closed. Second, for the vortex to reach a TC strength, the surface wind speed was not less than 17 m s⁻¹ and the vertical relative vorticity at 850 hPa was greater than 5×10^{-4} s⁻¹ at the same time. Third, the temperature within 1200 km radius from the detected vortex center was higher than 1 °C in the layer 300–500 hPa to ensure a warm-core structure. Finally, the TC lifespan should last at least for 3 days.

Spatial distribution of TCGF

Following our previous study[38], we defined TCGF at a grid point on a 1° by 1° resolution as the number of TCs generated in an area of 20° in longitude and 10° in latitude centered at a given grid point. This method transformed discrete genesis points into spatio-continuous records and resulted in a stable spatial relationship between the TCGF and related environmental and oceanic factors (Fig. 2). We chose a 20° ×10° box because the synoptic waves (such as equatorial Rossby waves, mixed Rossby–gravity waves, and easterly waves) and other types of synoptic disturbances that triggered TC genesis often have a zonal scale of about 2000 km and a meridional e-folded scale[48,49] of

about 1000 km. We also tested 30° × 15° and 10° × 5° domains. Generally, the result from a 30° × 15° domain shows a similar correlation with that using a 20° × 10° domain, while the correlations would contain much noise using a 10° × 5° domain. Here, the spatial correlation in TCGF between regression and observation is shown in Fig. 2a, b.

Reconstruction of 2023 SST anomalies with various climate modes

Based on the analysis, we posited that the JJASON-averaged SST anomalies in 2023 were contributed by a combination of factors: a strong El Niño event over the equatorial Pacific, a negative phase of PMM in the eastern Pacific, the record-breaking warming in the TNA, and an underlying background warming trend. Consequently, the SST anomalies (SSTA) can be reconstructed as follows:

$$SSTA^* = a \times Ni\tilde{n}o^* + b \times PMM^* + c \times TNA^* + d(GW)^* \times t \qquad (1)$$

where $SSTA^*$ is the reconstructed SSTA (Fig. 3b). Here, Niño*, derived from the regressed SST anomalies upon the normalized Niño index from 1980 to 2023, reflects the anomalous SST pattern attributed to ENSO (Supplementary Fig. 8a). Since the normalized Niño index in 2023 was 1.59 ($a = 1.59$), the SSTA in 2023 contributed by ENSO was defined as $a \times$ Niño*. The PMM* and TNA* components are similarly obtained, showing the regressed SSTA upon reversed PMM index (-PMM, Supplementary Fig. 8b) and TNA index (Supplementary Fig. 8c), respectively. With the normalized indices of the Niño, TNA and PMM, $a = 1.59$, $b = -2.03$, and $c = 2.5$. The coefficient d is the linear SST trend at each grid point, encapsulating the GW magnitude from 1980 to 2023. That means, the GW-related SST anomalies in 2013 could be approximated as $d(GW)^* \times t$ with $t = 44$. However, given the dependence of the linear trend on time period due to the influence of long-term climate variability, such as the Interdecadal Pacific Oscillation (IPO) and Atlantic Multidecadal Oscillation (AMO), we adjusted t by minimizing the disparity between the observed and reconstructed SST anomalies across the latitude between 45°S to 45°N.

$$Var = \min\left(\int_{45S}^{45N}\int_{0°}^{360°} (SSTA^* - SSTA)dxdy\right) \qquad (2)$$

We computed variance (Var) with t varying from 1 to 60 at 1-year interval and found that the least Var, and thus the most accurate reconstructed SSTA, occurred at $t = 30$ (Supplementary Fig. 12a, b). The bias between the observed ($SSTA$) and reconstructed ($SSTA^*$) SSTA averaged over 45°S to 45°N was about 0.37 °C ($Var=3312$), which was predominantly linked to the variability of the Kuroshio region over the Northwest Pacific and Atlantic. Further, the bias narrows to less than 0.2 °C in the tropical region between 15°S and 15°N. The GW increments with $t = 30$ is shown in Supplementary Fig. 4d, and the corresponding $SSTA^*$ reconstructed by the combination of the above four oceanic modes is given in Fig. 3b.

To accommodate uncertainties inherent in the GW magnitude due to the low-frequency climate variability, we further analyzed the linear trends of SSTs from 1960 to 2023 and from 1990 to 2023 (Supplementary Fig. 12c–f), respectively. We found that the linear trend of SST from 1960 to 2023 was slightly smaller than that from 1980 to 2023. This is because the former may be partly contributed by the negative IPO phase during 1980–2014. However, when $t = 37$ is chosen, the minimum variance between the observed and reconstructed SST anomalies can be achieved, with the SST bias of 0.47 °C, and the GW magnitudes based on 1980–2023 and 1960–2023 are similar. This is further verified by numerical experiments (Supplementary Fig. 13) based on the two slightly different SST warming magnitudes and spatial patterns (Supplementary Figs. 12b, 13d). The results show consistent contributions of TCGF by the two slightly different GW patterns (Supplementary Fig. 13). We found that the

linear trends from 1990 to 2023 was much larger mainly contributed by the negative SST anomalies in the negative phase of IPO. By comparing the magnitudes of variance based on different time periods (Supplementary Fig. 12a, c, e), we finally selected the time period 1980–2023 since the minimum variance is about 3312 (0.37 °C bias), considerably smaller than 4833 (0.47 °C bias) and 4412 (0.45 °C bias) based on the periods 1960–2023 and 1990–2023. This also highlighted that the choice of period could influence the perceived GW impact. Nevertheless, with the minimum variance based on the period 1980–2023, the reconstructed SSTA well captured the observed SSTA in 2023, offering a reasonable way to assess the relative importance of climate modes to the unprecedented TC activity over the NA and WNP in the strong El Niño year of 2023.

To validate the above reconstructed model, we constructed a sample-independent regression model of TCGF based on the leave-one-out method at each grid point using the PMM index, TNA index, ENSO index, and the normalized GW index derived from global averaged SST. We found a remarkable similar pattern between the regressed and observed TCGF (Fig. 2a, b), an increase over the NA and a basin-wide decrease over the WNP (Fig. 2c, d). The correlation coefficient between the sample-independent regression model and observation is 0.69 for the NA TCGF and 0.53 for the WNP TCGF (Fig. 2e, f). The sample-independent regression model confirms that the reconstructed SSTA based on the four oceanic modes can capture the observed SST anomalies and their contribution to TCGF anomalies over the NA and WNP in 2023.

Sensitivity experiments

In this study, we conducted a series of sensitivity experiments to unravel and quantify the disparate impacts of these oceanic modes on TCGF anomalies in the NA and WNP in 2023. Each experiment consists of 30 ensemble members, and each member is forced by different perturbed initial conditions with randomly small magnitudes. Here, we first conducted a climate run (CLIM Run) as a baseline, which was driven by climatological monthly SST during 1980–2022. The All Run with SSTs from the HadISST in 2023 and the surface air temperature used over lands was designed to reproduce the circulation and TCGF conditions in 2023. The Reconstruction Run was forced by the combination of climatological SST (CLIM Run) and the reconstructed SST anomalies using all four modes (PMM, TNA, ENSO, and GW; Fig. 3b). Note that the correlation between PMM and TNA is −0.4 as mentioned above. To avoid the PMM (TNA) impact on Atlantic (Pacific) SST anomaly, although the magnitude of the corresponding SST anomaly is small (Supplementary Fig. 8b, c), we constrained the PMM (TNA) induced SST anomalies only over the Pacific (Atlantic) region in the relevant experiments. We found that the TCGF anomalies over the WNP and NA were highly consistent in All Run and Reconstruction Run (Fig. 4a, b; contour vs shaded), which strongly suggests that the Reconstruction Run based on the four oceanic modes reproduced the main characteristics of TC activity in 2023. The No_ElNiño Run (Fig. 3c) mirrored the Reconstruction Run with the exclusion of the ENSO-related SST anomalies. Similarly, the No_GW Run paralleled the Reconstruction run, albeit without the influence of GW-related SST anomalies (Fig. 3d). The PMM_TNA Run was driven by the SST anomalies related to the PMM and TNA components (Fig. 3e). To further quantify the individual contributions by PMM and TNA on SST anomalies (Supplementary Fig. 8b, c), we conducted two additional experiments (PMM Run and TNA Run) to specifically focus on the PMM and TNA influences. As detailed above, the GW increment was derived based on the SST trend during 1980–2023 period. To test the sensitivity of the results to the uncertainty in GW increment, we also used the SST trends from 1960 to 2023 (Tr_60) and from 1990 to 2023 (Tr_90) (Supplementary Figs. 11 and 13) to conducted two additional experiments of Reconstruction Runs (Recon_Tr_60 and Recon_Tr_90 Runs) by substituting the original GW trends with Tr_60 and Tr_90. The

results from the two experiments were generally consistent, confirming that the GW was favorable for TC genesis over the NA while unfavorable for TC genesis over the WNP (Supplementary Fig. 13).

Statistic tests
In our statistical analysis, we calculated the degrees of freedom to ensure the robustness of our results. For the regression analysis covering the period from 1980 to 2023, the degree of freedom was established at 42. Meanwhile, the composite analysis, derived from the numerical experiments involving 60 ensemble members, was conducted with a higher degree of freedom, set at 58. To visually convey the significance of our results, p-values less than 0.1 are indicated by dots in Fig. 4.

Ethics statement
This research did not require the IRB approval because all the experiments depend on numerical simulations.

Data availability
In this study, the TC information data were downloaded from IBTrACS version 4 (https://www.ncei.noaa.gov/products/international-best-track-archive); the NCEP reanalysis data is obtained from https://downloads.psl.noaa.gov/Datasets/ncep.reanalysis.derived/pressure/; the ECMWF reanalysis data (https://cds.climate.copernicus.eu/cdsapp#!/dataset/reanalysis-era5-pressure-levels-monthly-means?tab=form) is used to verify the consistency; the SST data is derived from https://www.metoffice.gov.uk/hadobs/hadisst/data/download.html; the PMM index is from https://psl.noaa.gov/data/timeseries/monthly/PMM/pmmsst.data; the processed modeling experiments data[50], as well as the codes for plotting figures[50], have been deposited in the figshare database under accession code [https://figshare.com/s/2415440a2cd4cafee39a and https://figshare.com/ndownloader/files/47813770] with the identifiers https://doi.org/10.6084/m9.figshare.25217840.v1.

Code availability
In this study, the codes of python (version 3.9.12), ncl (version 6.6.2) and Intel Fortran (version 2021.10.0) for calculations and plotting figures[50] can be downloaded from figshare (https://figshare.com/s/2415440a2cd4cafee39a). An independent demo for testing python libraries that are used in this study can be downloaded from https://figshare.com/s/a89b67bc82105445a42c. The codes of python for statistics can be used on different platforms and can get the result in several minutes.

References
1. Li, K., Zheng, F., Zhu, J. & Zeng, Q.-C. El Niño and the AMO sparked the astonishingly large margin of warming in the global mean surface temperature in 2023. *Adv. Atmospheric Sci.* **41**, 1017–1022 (2024).
2. Patricola, C. M., Chang, P. & Saravanan, R. Degree of simulated suppression of Atlantic tropical cyclones modulated by flavour of El Niño. *Nat. Geosci.* **9**, 155–160 (2016).
3. Wang, B. & Chan, J. C. L. How Strong ENSO events affect tropical storm activity over the western North Pacific. *J. Clim.* **15**, 1643–1658 (2002).
4. Zhao, J. et al. Atmospheric modes fiddling the simulated ENSO impact on tropical cyclone genesis over the Northwest Pacific. *Npj Clim. Atmos. Sci.* **6**, 213 (2023).
5. Ham, Y.-G., Kug, J.-S., Park, J.-Y. & Jin, F.-F. Sea surface temperature in the north tropical Atlantic as a trigger for El Niño/Southern Oscillation events. *Nat. Geosci.* **6**, 112–116 (2013).
6. Yu, J., Li, T., Tan, Z. & Zhu, Z. Effects of tropical North Atlantic SST on tropical cyclone genesis in the western North Pacific. *Clim. Dyn.* **46**, 865–877 (2016).
7. Ham, Y., Kug, J. & Park, J. Two distinct roles of Atlantic SSTs in ENSO variability: North Tropical Atlantic SST and Atlantic Niño. *Geophys. Res. Lett.* **40**, 4012–4017 (2013).
8. Jiang, L., Li, T. & Ham, Y. Critical role of tropical North Atlantic SSTA in boreal summer in affecting subsequent ENSO evolution. *Geophys. Res. Lett.* **49**, e2021GL097606 (2022).
9. Gao, S., Zhu, L., Zhang, W. & Shen, X. Western North Pacific tropical cyclone activity in 2018: A season of extremes. *Sci. Rep.* **10**, 5610 (2020).
10. Wu, Q., Zhao, J., Zhan, R. & Gao, J. Revisiting the interannual impact of the Pacific Meridional Mode on tropical cyclone genesis frequency in the Western North Pacific. *Clim. Dyn.* **56**, 1003–1015 (2021).
11. Liu, C., Zhang, W., Stuecker, M. F. & Jin, F. Pacific Meridional Mode-western North Pacific tropical cyclone linkage explained by tropical Pacific Quasi-decadal variability. *Geophys. Res. Lett.* **46**, 13346–13354 (2019).
12. Gao, S., Zhu, L., Zhang, W. & Chen, Z. Strong modulation of the Pacific Meridional Mode on the occurrence of intense tropical cyclones over the western North Pacific. *J. Clim.* **31**, 7739–7749 (2018).
13. Zhang, W., Villarini, G. & Vecchi, G. A. Impacts of the Pacific Meridional Mode on June–August precipitation in the Amazon River Basin. *Q. J. R. Meteorol. Soc.* **143**, 1936–1945 (2017).
14. Zhao, J., Kug, J., Park, J. & An, S. Diversity of North Pacific Meridional Mode and its distinct impacts on El Niño-Southern Oscillation. *Geophys. Res. Lett.* **47**, e2020GL088993 (2020).
15. Zhang, W., Villarini, G., Vecchi, G. A. & Murakami, H. Impacts of the Pacific Meridional Mode on landfalling North Atlantic tropical cyclones. *Clim. Dyn.* **50**, 991–1006 (2018).
16. Huo, L., Guo, P., Hameed, S. N. & Jin, D. The role of tropical Atlantic SST anomalies in modulating western North Pacific tropical cyclone genesis. *Geophys. Res. Lett.* **42**, 2378–2384 (2015).
17. Zhang, W., Vecchi, G. A., Murakami, H., Villarini, G. & Jia, L. The Pacific Meridional Mode and the occurrence of tropical cyclones in the western North Pacific. *J. Clim.* **29**, 381–398 (2016).
18. Saji, N. H., Goswami, B. N., Vinayachandran, P. N. & Yamagata, T. A dipole mode in the tropical Indian Ocean. *Nature* **401**, 360–363 (1999).
19. Saji, N. & Yamagata, T. Possible impacts of Indian Ocean Dipole mode events on global climate. *Clim. Res.* **25**, 151–169 (2003).
20. Seager, R. et al. Strengthening tropical Pacific zonal sea surface temperature gradient consistent with rising greenhouse gases. *Nat. Clim. Change* **9**, 517–522 (2019).
21. Xie, S. Ocean warming pattern effect on global and regional climate change. *AGU Adv.* **1**, e2019AV000130 (2020).
22. Zhao, J., Zhan, R. & Wang, Y. Different Responses of tropical cyclone tracks over the western North Pacific and North Atlantic to two distinct sea surface temperature warming patterns. *Geophys. Res. Lett.* **47**, e2019GL086923 (2020).
23. Du, Y., Yang, L. & Xie, S.-P. Tropical Indian Ocean influence on Northwest Pacific tropical cyclones in summer following strong El Niño. *J. Clim.* **24**, 315–322 (2011).
24. Chiang, J. C. H. & Vimont, D. J. Analogous Pacific and Atlantic Meridional Modes of tropical atmosphere–ocean variability. *J. Clim.* **17**, 4143–4158 (2004).
25. Vimont, D. J., Battisti, D. S. & Hirst, A. C. Footprinting: A seasonal connection between the tropics and mid-latitudes. *Geophys. Res. Lett.* **28**, 3923–3926 (2001).
26. Xie, S.-P. & Philander, S. G. H. A coupled ocean-atmosphere model of relevance to the ITCZ in the eastern Pacific. *Tellus Dyn. Meteorol. Oceanogr.* **46**, 340 (1994).
27. Stuecker, M. F. Revisiting the Pacific Meridional Mode. *Sci. Rep.* **8**, 3216 (2018).

28. Amaya, D. J. The Pacific Meridional Mode and ENSO: A review. *Curr. Clim. Change Rep.* **5**, 296–307 (2019).
29. Ham, Y.-G. & Kug, J.-S. Role of north tropical atlantic SST on the ENSO simulated using CMIP3 and CMIP5 models. *Clim. Dyn.* **45**, 3103–3117 (2015).
30. Zhao, J., Zhan, R., Wang, Y., Xie, S.-P. & Wu, Q. Untangling impacts of global warming and Interdecadal Pacific Oscillation on long-term variability of North Pacific tropical cyclone track density. *Sci. Adv.* **6**, eaba6813 (2020).
31. Vimont, D. J. & Kossin, J. P. The Atlantic Meridional Mode and hurricane activity. *Geophys. Res. Lett.* **34**, 2007GL029683 (2007).
32. Patricola, C. M., Saravanan, R. & Chang, P. The impact of the El Niño–Southern Oscillation and Atlantic Meridional Mode on seasonal Atlantic tropical cyclone activity. *J. Clim.* **27**, 5311–5328 (2014).
33. Klotzbach, P. J. The influence of El Niño–Southern Oscillation and the Atlantic Multidecadal Oscillation on Caribbean tropical cyclone activity. *J. Clim.* **24**, 721–731 (2011).
34. Zhao, M., Held, I. M., Lin, S.-J. & Vecchi, G. A. Simulations of global hurricane climatology, interannual variability, and response to global warming using a 50-km resolution GCM. *J. Clim.* **22**, 6653–6678 (2009).
35. Murakami, H. et al. Detected climatic change in global distribution of tropical cyclones. *Proc. Natl Acad. Sci.* **117**, 10706–10714 (2020).
36. Murakami, H., Levin, E., Delworth, T. L., Gudgel, R. & Hsu, P.-C. Dominant effect of relative tropical Atlantic warming on major hurricane occurrence. *Science* **362**, 794–799 (2018).
37. Du, Y., Cai, W. & Wu, Y. A new type of the Indian Ocean Dipole since the mid–1970s. *J. Clim.* **26**, 959–972 (2013).
38. Song, K., Zhao, J., Zhan, R., Tao, L. & Chen, L. Confidence and uncertainty in simulating tropical cyclone long-term variability using the CMIP6-HighResMIP. *J. Clim.* **35**, 2829–2849 (2022).
39. Zhao, J., Zhan, R., Wang, Y. & Xu, H. Contribution of the interdecadal Pacific oscillation to the recent abrupt decrease in tropical cyclone genesis frequency over the western North Pacific since 1998. *J. Clim.* **31**, 8211–8224 (2018).
40. Henley, B. J. et al. A tripole index for the interdecadal Pacific oscillation. *Clim. Dyn.* **45**, 3077–3090 (2015).
41. Zhang, W. et al. Dominant role of Atlantic Multidecadal Oscillation in the recent decadal changes in western North Pacific tropical cyclone activity. *Geophys. Res. Lett.* **45**, 354–362 (2018).
42. Knapp, K. R., Kruk, M. C., Levinson, D. H., Diamond, H. J. & Neumann, C. J. The International Best Track Archive for Climate Stewardship (IBTrACS): Unifying Tropical Cyclone Data. *Bull. Am. Meteorol. Soc.* **91**, 363–376 (2010).
43. Knapp, K. R., Diamond, H. J., Kossin, J. P., Kruk, M. C. & Schreck, C. J. International Best Track Archive for Climate Stewardship (IBTrACS) Project, Version 4. NOAA National Centers for Environmental Information https://doi.org/10.25921/82TY-9E16 (2018).
44. Hersbach, H. et al. The ERA5 global reanalysis. *Q. J. R. Meteorol. Soc.* **146**, 1999–2049 (2020).
45. Kalnay, E. et al. The NCEP/NCAR 40-Year Reanalysis Project. *Bull. Am. Meteorol. Soc.* **77**, 437–471 (1996).
46. Rayner, N. A. et al. Global analyses of sea surface temperature, sea ice, and night marine air temperature since the late nineteenth century. *J. Geophys. Res. Atmos.* **108**, 2002JD002670 (2003).
47. Zhao, J. et al. How does tropical cyclone genesis frequency respond to a changing climate? *Geophys. Res. Lett.* **50**, e2023GL102879 (2023).
48. Chen, G. & Chou, C. Joint contribution of multiple equatorial waves to tropical cyclogenesis over the western North Pacific. *Mon. Weather Rev.* **142**, 79–93 (2014).
49. Feng, X., Yang, G.-Y., Hodges, K. I. & Methven, J. Equatorial waves as useful precursors to tropical cyclone occurrence and intensification. *Nat. Commun.* **14**, 511 (2023).
50. Zhao, Jiuwei (2024). Lapsed El Niño impact on Atlantic and Northwest Pacific tropical cyclone activity in 2023. figshare. Dataset. https://doi.org/10.6084/m9.figshare.25217840.v1.

Author contributions
J.Z., R.Z., Y.W., and S.X. conceived main parts of this study. J.Z. and R.Z. conducted the data analysis and numerical experiments. L.Z. and M.X. helped to post-process the modeling data. J. Z. plotted all the figures with improvements from L.Z. and two master students (F.W. and Z. W.). J.Z., R.Z., Y. W., S. X., L.Z. and M.X. proved and revised the manuscript.

Competing interests
The authors declare no competing interests.

Additional information
Supplementary information The online version contains supplementary material available at https://doi.org/10.1038/s41467-024-51241-9.

Correspondence and requests for materials should be addressed to Ruifen Zhan or Yuqing Wang.

Peer review information *Nature Communications* thanks Si Gao and the other, anonymous, reviewer for their contribution to the peer review of this work. A peer review file is available.

Reprints and permissions information is available at http://www.nature.com/reprints

Publisher's note Springer Nature remains neutral with regard to jurisdictional claims in published maps and institutional affiliations.